Available online at www.sciencedirect.com

SciVerse ScienceDirect

Ceramics International 39 (2013) 165–170

CERAMICS INTERNATIONAL

www.elsevier.com/locate/ceramint

# Effect of acids on the morphology and negative thermal expansion analysis of $ZrW_2O_8$ powders prepared by the hydrothermal method

Xiujuan Sun[a,*], Xiaonong Cheng[b], Juan Yang[b], Qinqin Liu[b]

[a]*Center of Analysis and Test, Jiangsu University, Zhenjiang 212013, Jiangsu, PR China*
[b]*School of Materials Science and Engineering, Jiangsu University, Zhenjiang 212013, Jiangsu, PR China*

Received 4 May 2012; received in revised form 1 June 2012; accepted 1 June 2012
Available online 13 June 2012

**Abstract**

Different acids were used to prepare $ZrW_2O_8$ powders at 570 °C by the hydrothermal method. The products were investigated by X-ray diffraction, scanning electron microscopy, transmission electron microscopy, high-resolution transmission electron microscopy, thermogravimetric and differential scanning calorimetry and Fourier transform infrared absorption spectra. The results indicate that among the chosen acids, only HCl and $HNO_3$ can be used to prepare pure $ZrW_2O_8$ powders with high crystallinity and rod-like shape. When the hydrothermal temperature reduces to 160 °C, nano-sphere particles with an average diameter of 30 nm is obtained, if prepared by $HNO_3$ addition. The results of in situ X-ray diffraction measurement indicate that $ZrW_2O_8$ powders prepared by pure HCl or $HNO_3$ have strong negative thermal expansion.


*Keywords:* $ZrW_2O_8$ powders; Negative thermal expansion; Nano-sphere; Hydrothermal method

## 1. Introduction

Most of the materials show positive thermal expansion when heated, but there are also some materials which contract with increasing temperature, such as $\beta$-eucryptite and $NaZr_2(PO_4)_3$. Those are named as negative thermal expansion (NTE) materials. Among them, cubic $ZrW_2O_8$ exhibits large isotropic negative thermal expansion property over its entire stability range from −272.3 °C to 777 °C [1–3]. The property has been attributed to low-energy vibration mode (also known as rigid unit modes—RUMs) [4–7] and the thermal expansion coefficient is $-8.7\times10^{-6}\,°C^{-1}$. Due to this anomalous behavior, $ZrW_2O_8$ has been attracted considerable interests both from the basic science and also from the potential technological application in the near-zero thermal expansion composite materials [3–9].

According to the phase diagram of the $ZrO_2$–$WO_3$ system [10], $ZrW_2O_8$ is thermodynamically stable only between 1105 °C and 1257 °C, which makes solid state reaction and the co-precipitation method [11] different to prepare pure powders. The sol–gel route [12–14] can reduce the heat-treatment temperature, but it needs a few weeks to prepare the precursor. Compared with them, the hydrothermal method [15] is becoming popular for its advantages, such as the use of mild temperature and pressure, production with nano-crystalline powders in one step, no high-temperature calcination and aggregate. In recent years, it has been reported on $ZrW_2O_8$ powders prepared by the hydrothermal method [15], but the research emphasis is on the influence of reaction conditions on the particle size, whereas the morphology control is not studied. It is well known that the particle shape is closely related with the property. At present, $ZrW_2O_8$ powders are usually used to prepare composite materials with irregular morphology. It can be believed that when the morphology of $ZrW_2O_8$ is controlled, it will be convenient to prepare composite materials to control the thermal expansion coefficient. In our previous research, it has been found that $ZrWMoO_8$ which belongs to the same NTE series could obtain different shapes by acid additions. In this paper, different acids are adopted to prepare $ZrW_2O_8$ powders by the hydrothermal method and the influence of

*Corresponding author. Tel.: +86 511 88792767.
*E-mail address:* zihesun@163.com (X. Sun).

0272-8842/$36.00 
http://dx.doi.org/10.1016/j.ceramint.2012.06.005

acids on the morphology and NTE property are also discussed.

## 2. Experimental

### 2.1. Synthesis of $ZrW_2O_8$ powders

Zirconium oxynitrate ($ZrO(NO_3)_2 \cdot 5\,H_2O$) and ammonium metatungstate ($N_5H_{37}W_6O_{24} \cdot H_2O$) were used as raw materials. The mole ratio of Zr and W was 1:2. After stirring over 2.5 h, different acids were added (the different acids used in the experiments in detail are shown in Table 1) and stirring was continued for another 3 h at 60 °C. Thereafter, a homogenous slurry was formed, and it was poured into a Teflon-lined Parr bomb and heated at 180 °C for 15 h. Then the product was filtered, washed with distilled water and dried at 60 °C. To obtain $ZrW_2O_8$ powders, the resulting precursor was heated at 570 °C for 6 h.

### 2.2. Characterization

The precursors were studied by thermogravimetric and differential scanning calorimetry using a Germany NETZSCH-STA449 C instrument with a heating rate of 10 °C $min^{-1}$ under nitrogen atmosphere. X-ray diffraction patterns were collected on a Rigaku D/max2500 diffractometer with Cu Kα ($\lambda = 0.15418$ nm) radiation with 40 kV/200 mA. In situ X-ray diffraction measurement was used to characterize the samples with a scan speed of $2°(2\theta)\ min^{-1}$ at room temperature, 100 °C, 125 °C, 150 °C, 175 °C, 200 °C, 300 °C, 400 °C, 500 °C, 600 °C and 700 °C. The lattice constants obtained at different temperatures were calculated by powder X software [16]. The morphologies were examined with PHILIPS XL-30ESEM (25 kV) and JSM-7001FE (40 kV) scanning electron microscopy. Transmission electron micrograph and high-resolution transmission electron micrograph were obtained on a PHILIPS TECNA I-12 (100 kV) transmission electron microscope. The Fourier transform infrared absorption spectra were recorded on a NICILET TFI-360 FTIR spectrometer.

## 3. Results and discussion

### 3.1. XRD and TG–DSC analysis

The XRD patterns of the precursors and the resulting powders are shown in Fig. 1 The XRD pattern of no. 1 precursor shown in Fig. 1 a is mainly amorphous which may be due to the weak acid of HAc, it is not strong enough to promote crystallization. After heating at 570 °C for 6 h, the pattern (Fig. 1b) exhibits only a few diffraction peaks which can be indexed to $WO_3$ (JCPDS 32-1395) with hexagon crystal structure. Seen from Fig. 1, the XRD patterns of the precursor and the resulting powders are almost the same for nos. 2 and 3 respectively. The patterns for no. 2 are in good agreement with that of $WO_3\ 2H_2O$ (JCPDS 18–1419) with tetragonal crystal structure and for no. 3 are indexed to $H_{0.23}WO_3$ (JCPDS 42-1261) with monoclinic crystal structure. However, the crystallinity is bad. This situation is due to the property of the acids. Tungstate has a strong condensation tendency in acidic solution and can occur dehydration condensation reaction easily to form polytungstate ion. When the acid is strong enough, the degree of condensation is great. Finally, hydrated tungsten trioxide can be formed, such as $HClO_4$ and $H_2SO_4$. In our reaction, tungstate undergoes condensation reaction to form $WO_3\ 2H_2O$ and $H_{0.23}WO_3$.

When the acid changes to $H_3PO_4$, the XRD pattern of no. 4 precursor can be indexed to $(NH_4)_3PW_{12}O_{40} \cdot 9.5H_2O$ (JCPDS 50-0305) shown in Fig. 1a. Because $PO_4^{3-}$ reacts firstly with ammonium metatungstate. After heating, the precursor decomposes and $W_{12}PO_{38.5}$ (JCPDS 41-0369) is obtained (Fig. 1b).

Compared with the standard JCPDS card, XRD patterns shown in Fig. 1a for the precursors of nos. 5 and 6 can be indexed to $ZrW_2O_7(OH)_2 \cdot (H_2O)_2$ (JCPDS 28-1500). To study the influence of HCl and $HNO_3$ addition on the thermal conversion behaviors of $ZrW_2O_7(OH)_2 \cdot (H_2O)_2$, the nos. 5 and 6 precursors are measured by TG–DSC (Fig. 2). In Fig. 2a, a well-defined mass loss of 7.2% in the temperature range of room temperature to 250 °C can be observed in the TG curve, reflecting an endothermic peak in the DSC curve which may be attributed to the transformation of $ZrW_2O_7(OH)_2 \cdot (H_2O)_2$ to amorphous $ZrW_2O_8$. There is a broad exothermic peak between 550 °C and 660 °C without obvious mass loss, which may be caused by the crystallization of $ZrW_2O_8$. In Fig. 2b, the endothermic peak and mass loss of 1.8% below 150 °C may be attributed to the volatilization of nitrogen oxides. There is about 7.3% mass loss centered at 275 °C which may also be caused by the transformation of $ZrW_2O_7(OH)_2 \cdot (H_2O)_2$ to amorphous $ZrW_2O_8$ with a relative endothermic peak. The exothermic reaction without mass loss from 560 °C to 610 °C may be ascribed to the crystallization of $ZrW_2O_8$ powders. The TG–DSC results indicate that no matter what the different acids are used, the heat-treatment temperature can retain the same. So we can choose 570 °C for 6 h to prepare $ZrW_2O_8$ powders.

Table 1
The relation between samples and different acids.

| Samples | No. 1 | No. 2 | No. 3 | No. 4 | No. 5 | No. 6 |
|---|---|---|---|---|---|---|
| Acid | HAc | $HClO_4$ | $H_2SO_4$ | $H_3PO_4$ | HCl | $HNO_3$ |

### 3.2. FTIR analysis

After heating at 570 °C for 6 h, the resulting powders are firstly analyzed by FTIR which is shown in Fig. 3 for no. 5. The main adsorption bands centered at 999, 913 and 872 $cm^{-1}$ are attributed to the symmetric stretching of $WO_4$ tetrahedra; those at 807 and 768 $cm^{-1}$ to asymmetric

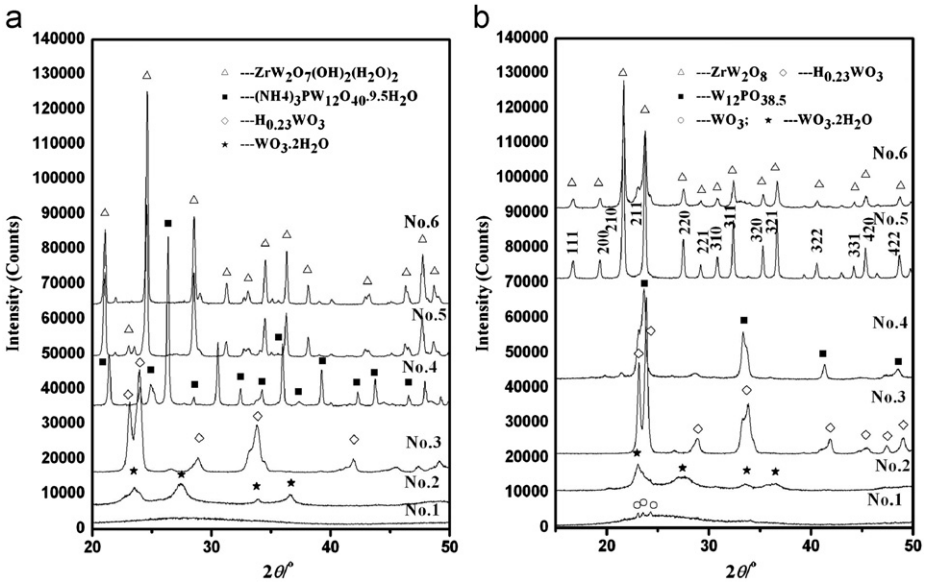


Fig. 1. XRD patterns of the precursors and resulting powders for different samples.

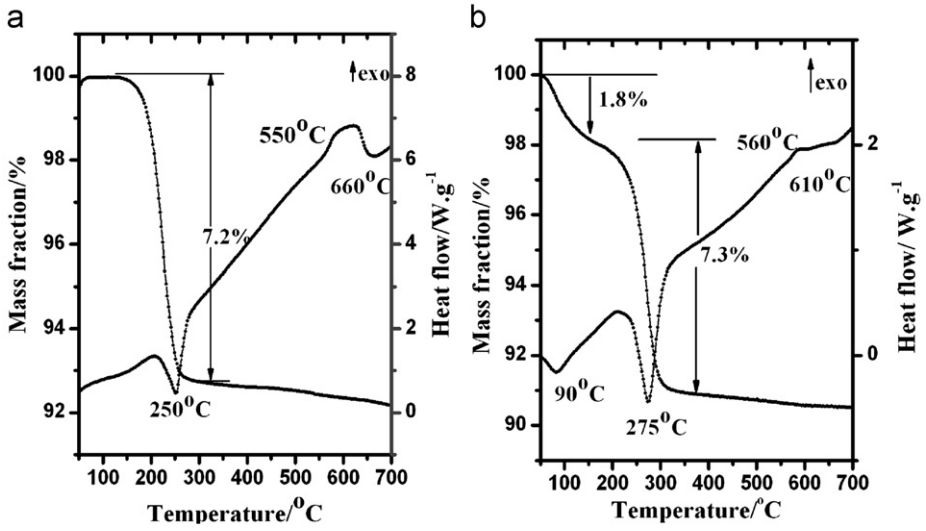


Fig. 2. TG–DSC curves of the precursors prepared by HCl (no. 5) and $HNO_3$ (no. 6) addition.

stretches; the broad structure band between 600 and 400 $cm^{-1}$ to $WO_4$ asymmetric bending modes, and $ZrO_6$ stretching modes are consistent with Ref. [1]. The results indicate that the resulting powder includes $WO_4$ and $ZrO_6$ function group. sample no. 6 also has the same result. The structure of nos. 5 and 6 are also characterized by XRD. The XRD patterns in Fig. 1b are the same, all the diffraction peaks are in good agreement with the JCPDS file of $ZrW_2O_8$ (JCPDS 50-1868) with cubic phase, and the sharp diffraction peaks manifest the high crystallinity. These results confirm the conclusions of TG–DSC and FTIR. From the above discussion, only certain acids can be used to form the precursors $ZrW_2O_7(OH)_2 \cdot (H_2O)_2$, which is an intermediate of the final product $ZrW_2O_8$ in the hydrothermal method. In this experiment, HCl and $HNO_3$ are suitable. The following will only discuss the powders prepared by HCl and $HNO_3$ addition.

### 3.3. Analysis of morphology

Fig. 4 shows the photographs of $ZrW_2O_8$ powders for nos. 5 and 6 heated at 570 °C for 6 h. It can be seen that the particles prepared by HCl and $HNO_3$ addition almost have the same shape, however, there are a few differences. It can be seen from Fig. 4a that the particles are homogeneously dispersed with a regular rod-like shape and an average dimension of 1.2 μm × 1.2 μm × 10 μm, the surface of the particles is smooth. Compared with that, the particles obtained by $HNO_3$ addition are mainly rod-like shape, but the length of the rod-like particles reduces while

the width maintains (Fig. 4b), and there are some small particles on the surface. The reason might be attributed to the different growth modes. We can assume that the powders prepared by $HNO_3$ addition may grow firstly to form small particles, then accumulate to form rod-like. This may be the reason for small particles existing on the surface.

In order to prove the above hypothesis, according to the classical hydrothermal crystal growth theory, the hydrothermal temperature is reduced to 160 °C to prepare powders by $HNO_3$ additions. After characterizing the sample, the resulting powders are in good agreement with that of $ZrW_2O_8$ (JCPDS 50-1868), the same as that in Fig. 1b. Fig. 4c shows the SEM photograph of $ZrW_2O_8$ powder by $HNO_3$ addition obtained at 160 °C. The particles are homogeneously dispersed with a regular nano-sphere and an average dimension of 30 nm. From this photograph, it can be confirmed that the assumption has a certain foundation and the specific theory will be studied in future. The crystal structure has also been studied by TEM and HRTEM in detail. Seen from Fig. 4d, the particles are aggregates, whereas, the shape and particle size are the same as the result of SEM. The right inset is the high magnification of the particle area in the image, the spacing between the fringes is 0.4106 nm corresponding to the lattice fringe created by lateral projection of the (210) planes of $ZrW_2O_8$.

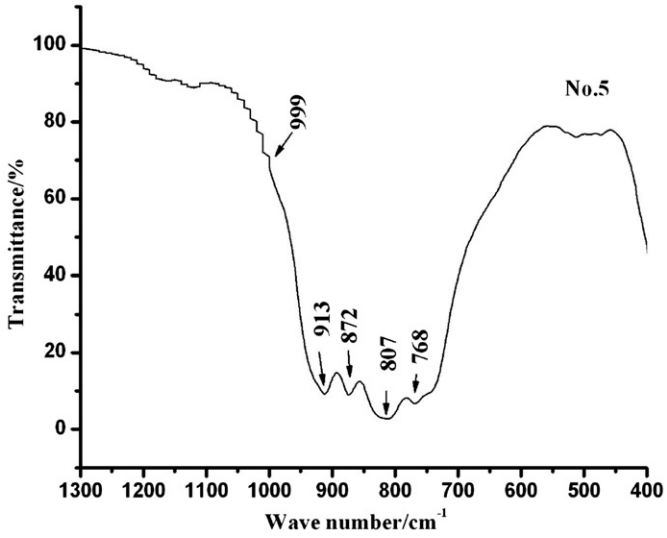


Fig. 3. FTIR spectra of $ZrW_2O_8$ powders prepared by HCl addition (no. 5).

### 3.4. Negative thermal expansion property analysis

Fig. 5 shows the XRD patterns at different temperatures of $ZrW_2O_8$ powders by HCl addition (Sample No. 5). In Fig. 5, the peaks slightly shift above $2\theta$ with an increasing temperature, which is obvious in the inset of Fig. 5. According to the Scherrer formula, when the structure is cubic, the diffraction angle increases, the value of $d$ decreases in contrast and so do the lattice constant. This

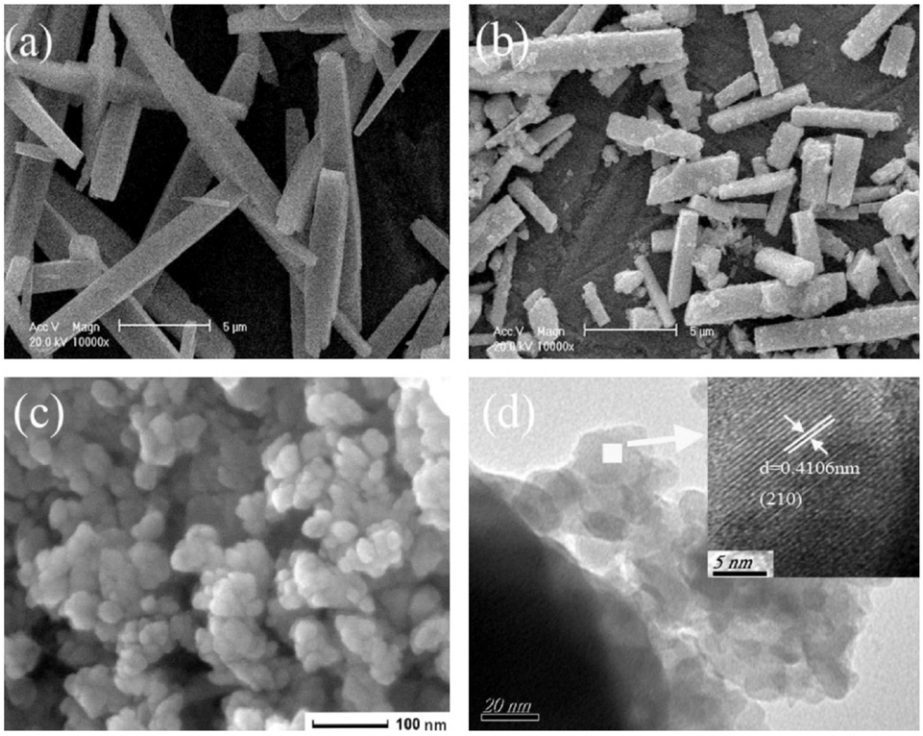


Fig. 4. Images of $ZrW_2O_8$ powders (a) SEM image for powders prepared by HCl addition (no. 5), (b) SEM image for powders prepared by $HNO_3$ addition (no. 6), (c) SEM image of powders prepared by $HNO_3$ addition obtained at 160 °C, and (d) TEM and HRTEM image of powders prepared by $HNO_3$ addition obtained at 160 °C.

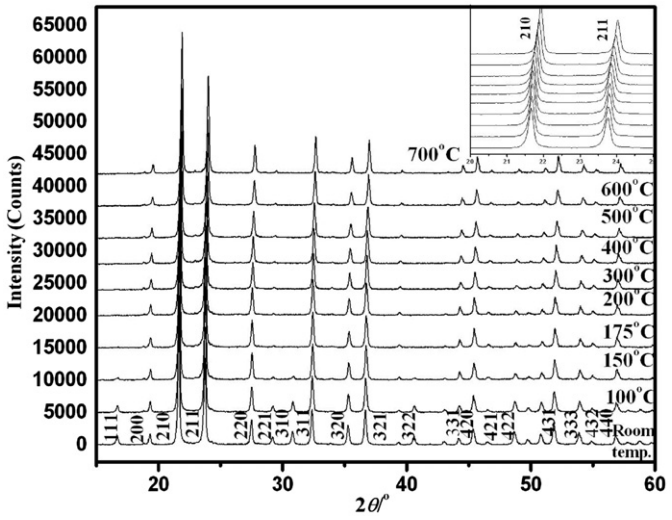


Fig. 5. XRD patterns at different temperatures of $ZrW_2O_8$ powders prepared by HCl addition (no. 5).

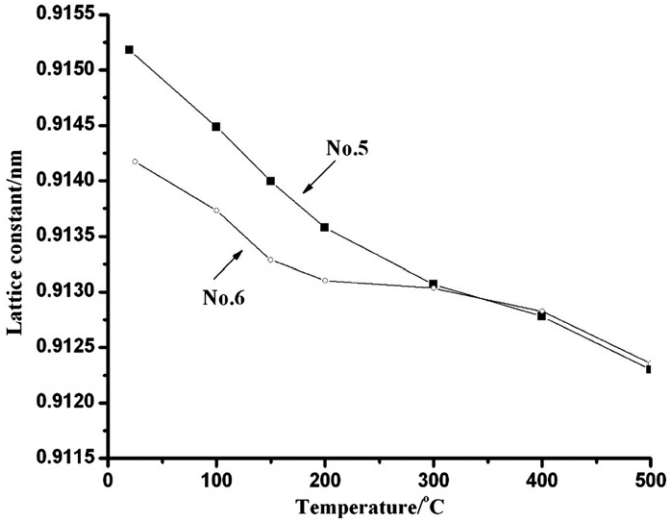


Fig. 6. The relation between lattice constants and temperatures.

indicates that the cell volume of $ZrW_2O_8$ is shrinking. The powder prepared by pure $HNO_3$ addition (no. 6) also exhibits a similar phenomenon.

Comparing the patterns characterized at 150 °C and 175 °C in Fig. 5, several diffraction peaks such as the (111), (310), (322), and (331) peaks that exist at low temperature disappear, and the (221) diffraction peak weakens, which is due to an $\alpha$–$\beta$ structure phase transition from an acentric phase to a centric phase. The low-temperature phase ($P2_13$) transits to the high temperature phase ($Pa\bar{3}$), which is considered to be order–disorder type [1–3,17]. The same result is also observed for sample no. 6.

Fig. 6 shows the relation between lattice constants and temperatures (nos. 5 and 6), which are calculated by the powder X software. The lattice constants decrease with increasing temperature. From the graph, the lattice constants of $\alpha$-$ZrW_2O_8$ for sample no. 5 are bigger than that of no. 6, whereas the lattice constants of $\beta$-$ZrW_2O_8$ are almost the same. After linear fitting, the thermal expansion coefficient of sample no. 5 is $-6.30\times10^{-6}\,°C^{-1}$ and $-3.66\times10^{-6}\,°C^{-1}$ for sample no. 6 from room temperature to 500 °C. The thermal expansion coefficients are $-9.89\times10^{-6}\,°C^{-1}$ and $-7.64\times10^{-6}\,°C^{-1}$ for $\alpha$ and $\beta$ structure phases of sample no. 5, respectively. The thermal expansion coefficients are $-7.36\times10^{-6}\,°C^{-1}$ and $-2.71\times10^{-6}\,°C^{-1}$ for $\alpha$ and $\beta$ structure phases of sample no. 6, respectively.

## 4. Conclusion

Different acids are used to prepare $ZrW_2O_8$ powders. Among the chosen acids, only HCl and $HNO_3$ can be adopted to synthesize powders and the resulting $ZrW_2O_8$ products are pure with good crystallization and mainly rod-like shape. When the hydrothermal temperature reduces to 160 °C, nano-sphere particles with an average dimension of 30 nm are obtained when pure $HNO_3$ is added. The results of in situ X-ray diffraction measurement indicate that $ZrW_2O_8$ powders have strong negative thermal expansion property, the average thermal expansion coefficients of $ZrW_2O_8$ powders prepared by pure HCl and $HNO_3$ addition are $-6.30\times10^{-6}\,°C^{-1}$ and $-3.6\times10^{-6}\,°C^{-1}$ from room temperature to 500 °C, respectively.

## Acknowledgment

The authors thank the Nation Natural Science Foundation of China (no. 50372027) the Postdoctoral Science Foundation (1143001059) and the Research Initiation Fund (1283300001) of Jiangsu University.

## References

[1] J.S.O. Evans, T.A. Mary, T. Vogt, M.A. Subramanian, A.W. Sleight, Negative thermal expansion in $ZrW_2O_8$ and $HfW_2O_8$, Chemistry of Materials: A Publication of the American Chemical Society 8 (1996) 2809–2823.
[2] J.S.O. Evans, T.A. Mary, A.W. Sleight, Negative thermal expansion in a large molybdate and tungstate family, Journal of Solid State Chemistry 133 (1997) 580–583.
[3] T.A. Mary, J.S.O. Evans, T. Vogt, A.W. Sleight, Negative thermal expansion from 0.3–1.50 K in $ZrW_2O_8$, Science 272 (1996) 90–92.
[4] A.W. Sleight, A. Rev, Isotropic negative thermal expansion, Materials Science 28 (1998) 29–43.
[5] A.K.A. Pryde, K.D. Hammonds, M.T. Dove, V. Heine, J.D. Gale, M.C. Warren, Origin of the negative thermal expansion in $ZrW_2O_8$ and $ZrV_2O_7$, Journal of Physics: Condensed Matter 8 (1996) 10973–10982.
[6] A.K.A. Pryde, K.D. Hammonds, M.T. Dove, V. Heine, J.D. Gale, M.C. Warren, Rigid unit modes and the negative thermal expansion in $ZrW_2O_8$, Phase Transitions 61 (1997) 141–153.
[7] J.Z. Tao, A.W. Sleight, The role of rigid unit modes in negative thermal expansion, Journal of Solid State Chemistry 173 (2003) 442–448.
[8] C. Lind, D.G. VanDerveer, A.P. Wilkinson, J.H. Chen, M.T. Vaughan, D. Weidner, New high-pressure form of the negative thermal expansion materials zirconium molybdate and hafnium molybdate, Journal of Materials Chemistry 13 (2001) 487–490.

[9] C.A. Perottoni, J.E. Zorzi, J.A.H. Jornada, Entropy increase in the amorphous-to-crystalline phase transition in zirconium tungstate, Solid State Communications 134 (2005) 319–322.
[10] L.L.Y. Chang, M.G. Scroger, B. Philips, Condensed phase relations in the systems $ZrO_2$–$WO_2$–$WO_3$ and $HfO_2$–$WO_2$–$WO_3$, Journal of the American Ceramic Society 50 (1967) 211–215.
[11] U. Kameswari, A.W. Sleight, J.S.O. Evans, Rapid synthesis of $ZrW_2O_8$ and related phase, and structure refinement of $ZrWMoO_8$, International Journal of Inorganic Materials 2 (2000) 333–337.
[12] C. Lind, A.P. Wilkinson, Seeding and the non-hydrolytic sol–gel synthesis of $ZrW_2O_8$ and $ZrMo_2O_8$, Journal of Sol–Gel Science and Technology 25 (2002) 51–56.
[13] A.P. Wilkinson, C. Lind, S. Pattanaik, A new polymorph of $ZrW_2O_8$ prepared using nonhydrolytic sol–gel chemistry, Chemistry of Materials: A Publication of the American Chemical Society 11 (1999) 101–108.
[14] L.D. Noailles, H.H. Peng, J. Starkovich, B. Dunn, Thermal expansion and phase formation of $ZrW_2O_8$ aerogels, Chemistry of Materials: A Publication of the American Chemical Society 16 (2004) 1252–1259.
[15] X.R. Xing, Q.F. Xing, R.B. Yu, J. Meng, J. Chen, G.R. Liu, Hydrothermal synthesis of $ZrW_2O_8$ nanorods, Physica B—Condensed Matter 371 (2006) 81–84.
[16] C. Dong, Powder X: Windows-95-based program for powder X-ray diffraction data procession, Journal of Applied Crystallography 32 (1999) 838–838.
[17] Y. Yasuhisa, T. Toshihide, S. Kazuya, S. Michio, Heat capacity and order–disorder phase transition in negative thermal expansion compound $ZrW_2O_8$, Journal of Chemical Thermodynamics 36 (2004) 525–531.